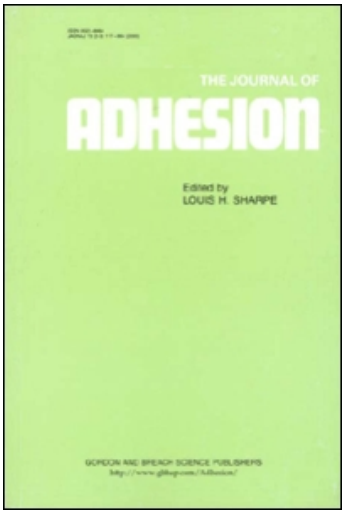

The Journal of Adhesion
Publication details, including instructions for authors and subscription information:
http://www.informaworld.com/smpp/title~content=t713453635

Quantification of Coating Adhesion Using Laser Induced Decohesion Spectroscopy

J. S. Meth[a]; D. Sanderson[a]; C. Mutchler[a]; S. J. Bennison[a]
[a] DuPont Co., Central Science and Engineering, Wilmington, DE, USA

To cite this Article Meth, J. S. , Sanderson, D. , Mutchler, C. and Bennison, S. J.(1998) 'Quantification of Coating Adhesion Using Laser Induced Decohesion Spectroscopy', The Journal of Adhesion, 68: 1, 117 — 142
To link to this Article: DOI: 10.1080/00218469808029582
URL: http://dx.doi.org/10.1080/00218469808029582

J. Adhesion, 1998, Vol. 68, pp. 117 - 142
Reprints available directly from the publisher
Photocopying permitted by license only

Quantification of Coating Adhesion Using Laser Induced Decohesion Spectroscopy

J. S. METH*, D. SANDERSON, C. MUTCHLER and S. J. BENNISON

DuPont Co., Central Science and Engineering, P. O. Box 80328, Wilmington, DE 19880-0328, USA

(Received 19 August 1997; In final form 16 December 1997)

We present a new technique, laser induced decohesion spectroscopy (LIDS), which is capable of measuring the practical work of adhesion G between a transparent polymer coating and an opaque coating or substrate. In LIDS, a laser pulse directed onto the sample creates a blister at the transparent/opaque interface. The blister's internal pressure depends on the laser pulse energy, and at a critical pressure the sample fractures, creating an annular debond similar to that obtained in the standard blister test. By measuring physical variables such as the curvature of the blister, and its radius and thickness, it is possible to deduce G. Here we measure G between an automotive clearcoat and four opaque basecoats of various pigmentations (black, white, red, metallic green) as a function of clearcoat thickness. We find that G depends on pigmentation due to the various pigment volume concentrations (PVC's) and specific pigment-binder interactions. Also, G depends on the clearcoat thickness when the thickness is comparable with the size of the plastic zone, R_p.

Keywords: Practical work of adhesion; transparent polymer coating; opaque substrate; automotive coatings; blister test; debonding by pulsed IR laser; laser induced decohesion spectroscopy (LIDS); blister curvature and internal blister pressure; modeling; theory; experiment

INTRODUCTION

Coatings are inherent to many technologies, from paint systems to electronics manufacturing [1 - 3]. One of the parameters that needs to be known is the adhesion, or resistance to fracture, of a coating to a

*Corresponding author.

substrate or to another coating. In general, it is difficult to quantify this adhesion. Many qualitative methods are available, such as the crosshatch-peel test and the x-hatch test for paints. Quantitative methods include instrumented peel tests, double cantilever beam methods, and blister tests. These techniques require special sample preparations, which makes them difficult to apply to paint adhesion.

We are concerned here with quantifying the adhesion between successive layers of paint, or between paint and a substrate. Currently, the adhesion is qualitatively measured using the crosshatch-peel test. It is quick and easy, and the results correlate with field tests. The disadvantage is that many modern coating systems can easily pass this test, yet there can be substantial differences in the adhesion, which may only become manifest when the sample is subjected to environmental stresses such as accelerated aging. As technology advances, the ability of the crosshatch-peel test to discriminate between good and excellent coating adhesion diminishes. In this sense the crosshatch-peel test has a limited dynamic range. There has long been a need for a more quantitative test method.

We have developed laser induced decohesion spectroscopy (LIDS) to quantify the adhesion in such systems. This paper presents the technique and some of the more basic results we have obtained so far. LIDS is essentially a new modification of the blister test [4–10]. In the blister test, it is necessary to generate pressure to produce a blister. This has led in the past to very ingenious ways to introduce that pressure. Unfortunately, the preparation of the samples became that much more complicated. LIDS employs photothermal ablation as the mechanism for generating internal pressure. Generally in photothermal ablation, a high power, temporally short, laser pulse incident on an opaque material causes it to heat up extremely rapidly, whereupon bonds break in that material, producing gases that expel from the surface. If a transparent layer covers the opaque one, the ablation process produces an internal pressure. In our experimental configuration, Figure 1, the opaque polymer is ablated, and a pressure is generated between the opaque and transparent polymers. The close proximity of a rigid substrate prevents significant deformation of the opaque layer, but the experiment still works with a coating on a deformable substrate. This internal pressure deforms the transparent coating, producing a blister directly above the ablated area. By

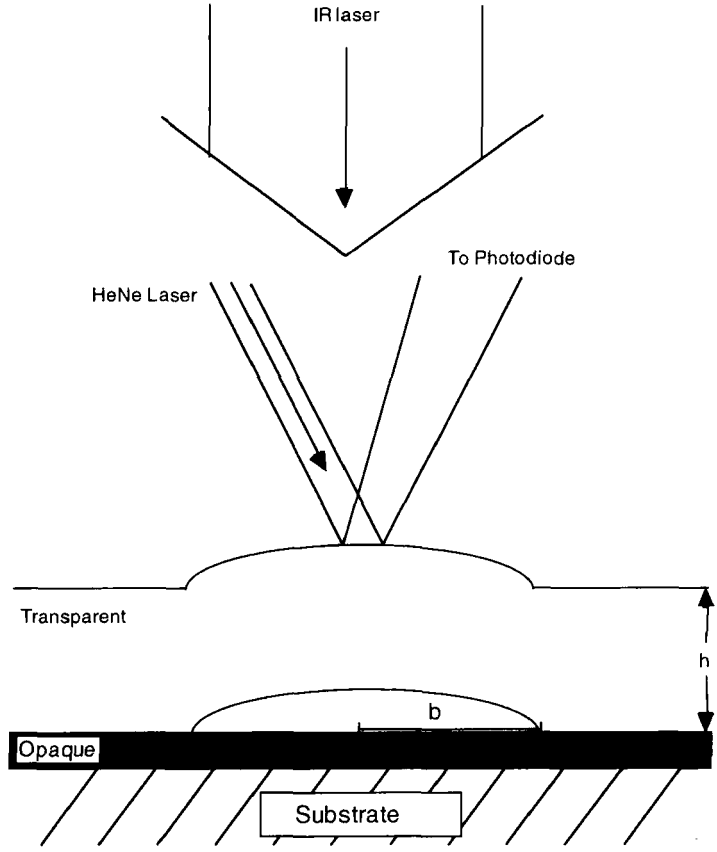

FIGURE 1 Schematic of LIDS experiment. An IR laser pulse creates a blister, while a HeNe beam probes the curvature of the surface.

measuring the curvature of the blister at its top, center, the internal pressure of the blister can be known. By itself, this process does not involve any debonding between the two layers outside of the ablated region. This is analogous to the small initial debond or hole that is necessary in the standard blister test. As the laser pulse energy is increased, more ablation occurs, and the internal pressure increases along with the associated strain energy stored in the system. At some critical laser pulse energy, the Griffith criterion for crack propagation [11] is exceeded, and the blister expands radially into the region of the

sample that was not ablated, producing an annular debond area, similar to other blister tests. At this critical laser pulse energy, there exists a critical internal pressure which is related to the work of adhesion. While we refer to the practical work of adhesion as G in this paper, it should be understood that these values are strongly influenced by dissipative processes in the coatings, and are not a measurement of any purely interfacial property.

There are several advantages to the LIDS technique. Foremost, the geometry of the LIDS experiment allows testing of film systems without special sample preparation-no holes need to be drilled, no other substrates need to be attached. Second, the initiating laser pulse controls the fracture rate. The rise time of the blister is ~ 1 μs. At these rates, the response of the polymer is determined by the glassy modulus, and viscous effects are not important during the blister creation. The values measured by LIDS are applicable to the problem of chipping of paint by stones. Third, the pressures generated by the ablation process can easily be in excess of 100 MPa, allowing large values of adhesion to be measured ($1-1000$ J/m^2).

EXPERIMENT

In LIDS (see Fig. 1), the typical sample consists of a transparent polymer coating on top of an opaque polymer coating, supported by a rigid substrate (similar to the fender on an automobile). LIDS can also be performed on samples consisting of a transparent polymer covering an opaque substrate (such as primer on thermoplastic olefin, a major automotive structural material, or polyimide on copper). An IR laser pulse impinges on the sample, passing through the transparent layer and ablating a portion of the opaque layer. This produces the blister. A separate, continuous-wave Helium-Neon (HeNe) laser reflects from the surface of the blister. The experimental observable is the intensity of HeNe laser light that passes through a circular aperture of known diameter. This intensity is related to the diameter of the laser beam. When a laser reflects from a positively-curved surface, the laser beam diverges so its diameter increases. Thus, we relate the laser intensity passing through the aperture to the radius of curvature of the blister.

There is a critical laser pulse energy in the LIDS experiment,

corresponding to a critical internal blister pressure. At energies below critical, the laser pulse ablates a portion of the opaque material, creating a blister in the transparent material directly above it. This is the starter crack that is necessary in all fracture mechanics experiments. At energies above critical, in addition to the starter crack, an annular debond is created around the ablation site. The sample has fractured. The critical energy is the point of interest. At this energy, the pressure created by the laser pulse is just enough to begin crack propagation. The generated pressure is stored as strain energy in the blister. At the critical energy, the strain energy in the system is maximized, and any further accommodation of mechanical deformation is performed by creating new surfaces, initiating a crack. At this critical energy, the top surface of the blister is curved, and it is this curvature that we are interested in knowing.

First we need to find this critical laser pulse energy for a given sample. This is done by exposing the sample to a laser pulse of a given energy many times (usually ten) and examining the resulting blisters under a microscope. For energies below critical, no cracks are visible under the microscope. Above the critical energy, an annular debond can be seen. Reiterating this process eventually yields the critical energy, to $\pm 5\%$. It is noted here that for strongly adhering systems, as the laser energy continues to exceed the critical energy, the debond turns into a classic cone crack, finally resulting in the ejection of a frustum-shaped chip from the system. For weakly adhering systems, the crack stays at the interface, and the annular area continues to increase.

Once the critical laser pulse energy is obtained, we then need to measure the radius of curvature of the blister at this energy. This is done by exposing the sample to a range of laser pulse energies spanning from the threshold energy, at which a blister may just be detected, up to the critical energy, where crack propagation begins, and measuring the curvature of the blister for every exposure. In this range of energies, there is no fracture in the sample. The ablation process produces the starter crack, and we measure the radius of curvature associated with each ablation. It is important to realize that LIDS is a single-shot experiment. One laser pulse impinges on one location of the sample. The sample is then moved to a fresh spot before another laser pulse hits the sample. When one plots the

measured curvature *versus* the laser pulse energy, a linear relationship is observed, and this is fitted to a line. We then extrapolate this line to the critical laser pulse energy to deduce the curvature (see Fig. 4).

It is necessary to know the thicknesses of the coatings. To do this, a small section of the plate is cut and polished in cross-section. The thicknesses are measured under a microscope with a calibrated reticle, reducing the standard error to $\pm 1\%$. The microscope is similarly used to measure the radii of the blisters at the critical laser pulse energy.

The ablating laser pulse is produced by a cavity-dumped regenerative oscillator running at 10 Hz, pumped by a CW, mode-locked Nd:YLF laser ($\lambda = 1.053$ μm, pulsewidth 50 ps). The output energy is stable to $\pm 3\%$, after the beam is cleaned up by a vacuum spatial filter. A shutter system isolates a single pulse. The laser is then focused onto the sample to a $1/e^2$ intensity radius of 50 μm; thus, the blisters tend to have radii of this dimension. The sample itself is mounted vertically at the focal plane of the IR laser pulse on a motorized translation stage which can be positioned reproducibly to 1 μm *via* computer control. A blister is formed by exposing the sample to a single IR laser pulse, and recording the reflected HeNe intensity on a digital oscilloscope (LeCroy 9374M). The scope trace is imported to a computer and analyzed to extract the curvature. The sample is then translated 1 mm before another laser pulse is incident on the sample. No position on the sample is ever exposed to more than a single laser pulse for data acquisition. The focused spot size of the HeNe laser is $1/e^2$ intensity radius of 25 μm.

The samples were prepared by standard techniques for automotive panels. The substrates were $4'' \times 12''$ (10.2×30.5 cm) phosphated cold-rolled steel panels with electrocoat and primer layers. The opaque basecoat was hand sprayed to a dry thickness of ~25 μm (1 mil). Four different basecoat colors were tested: black, white, red, and metallic green. The metallic aspect of the green paint comes from aluminum flakes dispersed in the formulation. These were water borne basecoats, consisting of a latex and melamine/formaldehyde resin, along with pigment, dispersant, and rheology control agents. The basic chemistry was the same for the coatings. The pigment volume concentration (PVC) was 2% for black, 15% for red 7% for green (4% of which is the aluminum flakes), and 21% for white. The panels were sprayed in a vertical orientation with a clearcoat (a crosslinking acrylic polymer) on

an automatic spraying machine and cured horizontally. Different film builds were prepared for each basecoat to examine the effect of clearcoat thickness on the experiment. This enabled us to study the effect of plastic zone size on coating adhesion.

THEORY

The theoretical analysis of the LIDS experiment consists of three links between four parameters. First, Gaussian beam propagation theory is used to relate the measured spot size of the HeNe laser beam reflected from the blister to its radius of curvature. Next, the biharmonic equation for the mechanical deformation in a model system is solved by expanding the stress potential function in a series to the sixth order, and choosing appropriate boundary conditions to solve for the prefactors. From this analysis we are able to relate theoretically the curvature of the blister to the internal pressure. We are also able to calculate the strain energy in the system, which is similar to the far-field energy described by Andrews [7]. Finally, by applying Griffith's criterion for crack propagation, we are able to relate the internal pressure to the adhesion parameter G, which is the material property of interest.

A. Relating Laser Spot Size to Blister Curvature

To measure the curvature of the blister, we measure the intensity of light that passes through a circular aperture placed in the beam path of the HeNe laser. The curvature is extracted by solving the complex algebraic equations for Gaussian beam propagation through the system [12]. This calculation is detailed in Appendix A. The result is an algebraic formula which is integrated into the computer program that controls data transfer from the oscilloscope. Thus, once an oscilloscope trace is transferred, the corresponding curvature is immediately calculated.

B. Relating Blister Curvature to Internal Blister Pressure

To relate the curvature to the internal blister pressure, applicable for any laser pulse energy, we create a theoretical model which consists of

a thick, circular disk, to which a uniform pressure, q, is applied at the lower surface. We use this as the model for the blister, and solve the problem using stress potential functions [13]. This solution includes stretching and bending of the disk. To account for the fact that the blister is part of a larger system, we apply various boundary conditions at the edge of the model disk. We begin with a circular disk of radius b and thickness h, diagrammed in Figure 2. The origin is taken at the center. We wish to solve the biharmonic operator for the boundary conditions of interest. The following equations represent the equation for the stress potential function, ϕ, and the expressions for stresses and displacements, where u is the radial displacement and w is the normal displacement:

$$\nabla^2\nabla^2\phi = 0 \tag{1a}$$

$$\sigma_r = \frac{\partial}{\partial z}\left(\nu\nabla^2\phi - \frac{\partial^2\phi}{\partial r^2}\right) \tag{1b}$$

$$\sigma_\theta = \frac{\partial}{\partial z}\left(\nu\nabla^2\phi - \frac{1\partial\phi}{r\partial r}\right) \tag{1c}$$

$$\sigma_z = \frac{\partial}{\partial z}\left((2-\nu)\nabla^2\phi - \frac{\partial^2\phi}{\partial z^2}\right) \tag{1d}$$

$$\tau_{rz} = \frac{\partial}{\partial z}\left((1-\nu)\nabla^2\phi - \frac{\partial^2\phi}{\partial z^2}\right) \tag{1e}$$

$$2Gw = 2(1-\nu)\nabla^2\phi - \frac{\partial^2\phi}{\partial z^2} \tag{1f}$$

$$2Gu = -\frac{\partial^2\phi}{\partial r\partial z} \tag{1g}$$

We expand ϕ in a series, inclusive to terms that describe quartic displacements:

$$\begin{aligned}\phi =& a_3(2z^3 - 3r^2z) + b_3(r^2z + z^3) \\ &+ a_4(8z^4 - 24r^2z^2 + 3r^4) + b_4(2z^4 + r^2z^2 - r^4) \\ &+ a_6(16z^6 - 120z^4r^2 + 90z^2r^4 - 5r^6) \\ &+ b_6(8z^6 - 16z^4r^2 - 21z^2r^4 + 3r^6) \end{aligned} \quad (2)$$

Equation (2) is substituted into Eqs. (1a–1g), and the appropriate boundary conditions are applied to solve for the coefficients. There are four elementary boundary conditions that are common to all the solutions: 1) $\sigma_z = 0$ for $z = h/2$ – there is no normal force acting at the upper, free surface; 2) $\sigma_z = -q$ for $z = -h/2$ – there is a uniform compressive force, q, acting at the lower surface; 3–4) $\tau_{rz} = 0$ for $z = \pm h/2$ – there are no shear forces at the upper or lower surfaces. We are assuming that the ablation process produces a uniform pressure on the lower surface of the blister.

In addition to these four, two more conditions are needed. In the simply-supported case, the blister is constrained to have no net bending moments along the outside edge, and to have its neutral plane in the center of the disk. In the rigidly-clamped scenario, the radial displacement of the blister is zero at its upper and lower edges. These

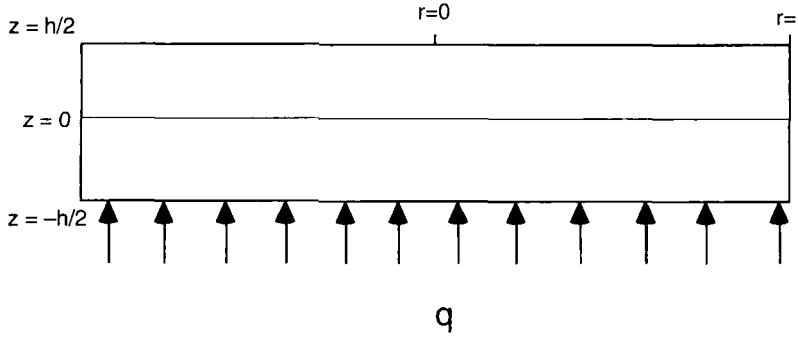

FIGURE 2 Diagram of theoretical model of a thick disk of radius b, thickness h, with a uniform pressure, q, applied to the bottom surface.

two boundary conditions represent opposite extremes of clamping, which provides limits for the possible variations in the theory. In addition to these two cases, a mixed boundary condition is examined. In this case, the radial displacement at the bottom edge of the disk is zero, while the radial stress at the top edge of the disk is zero. It turns out that in the rigidly-clamped case, the radial stress is zero at the point $r/b = [(1 + \nu)/(3 + \nu)]^{1/2}$. The mixed boundary conditions case merely extends that zero point out further on the disk, to $r/b = 1$, allowing some radial displacement at the upper edge. This case is then intermediate to the first two. The prefactors are collected together in Table I, normalized by the pressure, q. Along with these solutions, we also examine the textbook solutions for a thin disk and a thick disk [14]. As will be shown below, the choice of boundary conditions does not have an extreme effect on the results. In addition to the quantities described in Eq. (1), the analytic solution enables us to derive expressions for the strains, tensor invariants, and combinations thereof, most notably the hydrostatic pressure, the deformational stress, and the strain energy density.

For all cases, the relationship between pressure and curvature may be summarized by:

$$q = \frac{16D}{R_c b^2 s(h/b)} \tag{3a}$$

$$s(h/b) = k_1 + k_2(h/b)^2 \tag{3b}$$

$$D = \frac{Eh^3}{12(1 - \nu^2)} \tag{3c}$$

D is the flexural rigidity of the clear coat, E is the modulus, ν is Poisson's ratio, h is the thickness, b is the blister radius, R_c is the measured radius of curvature, and k_1 and k_2 are constants depending on the particular boundary conditions, summarized in Table II. From this analysis, we can relate the curvature calculated at the critical laser pulse energy to the critical internal blister pressure. This pressure is

TABLE I Coefficients for ϕ, normalized by the pressure, q

	Simply supported	*Rigidly clamped*	*Mixed*
a_3	$\frac{(5\nu-1)}{60(\nu+1)}$	$\frac{1}{60(\nu-1)}$	$\frac{3(\nu-1)(5\nu-7)b^2-4(\nu+1)h^2}{240(1-\nu^2)h^2}$
b_3	$\frac{-1}{20(\nu+1)}$	$\frac{1}{20(\nu-1)}$	$-\frac{3(\nu-1)b^2+2(\nu+1)h^2}{40(1-\nu^2)h^2}$
a_4	$\frac{5(-7\nu^2-13\nu+24)b^2+(7\nu^2-64\nu-11)h^2}{4480(1+\nu)h^3}$	$\frac{-3(\nu-1)(7\nu-8)b^2+(7\nu^2-22\nu+13)h^2}{2688(\nu-1)h^3}$	$\frac{3(\nu-1)(\nu+2)(7\nu-8)b^2-(\nu+1)(7\nu^2-22\nu+13)h^2}{2688(1-\nu^2)h^3}$
b_4	$\frac{15(3+\nu)b^2+3(3-\nu)h^2}{560(1+\nu)h^3}$	$\frac{3(1-\nu)b^2+(1+\nu)h^2}{112(1-\nu)h^3}$	$\frac{3(\nu+2)(1-\nu)b^2+(1+\nu)^2h^2}{112(1-\nu^2)h^3}$
a_6	$\frac{(18-11\nu)}{10560h^3}$	$\frac{(18-11\nu)}{10560h^3}$	$\frac{(18-11\nu)}{10560h^3}$
b_6	$\frac{1}{352h^3}$	$\frac{1}{352h^3}$	$\frac{1}{352h^3}$

TABLE II Summary of parameters for $s(h/b)$

Theory	k_1	k_2
clamped thin plate	1	0
simply supported disk	$\frac{(3+\nu)}{(1+\nu)}$	$\frac{4(2+\nu)}{5(1+\nu)}$
clamped disk	1	$\frac{2(2-\nu)}{3(1-\nu)}$
mixed b.c. disk	$\frac{(2+\nu)}{(1+\nu)}$	$\frac{2(2-\nu)}{3(1-\nu)}$
clamped thick plate	1	$\frac{2}{(1-\nu)}$

then related to the practical work of adhesion, or resistance to fracture.

C. Relating Critical Internal Blister Pressure to Practical Work of Adhesion

Once the internal blister pressure is known, relating it to G is straightforward, following the literature analysis using linear elastic fracture mechanics. The total strain energy in the system is split into two terms, near-field and far-field, following Andrews [7]. The near-field energy is that associated with the crack tip, and is available from textbooks [15]. The far-field energy is associated with strain energy stored away from the crack tip, namely in the blister and in the opaque material that comprises the elastic foundation. From the solutions derived for the thick disk, we can calculate the strain energy in the blister. Upon equating G with dU/dA, where U is the strain energy and A is the crack area, we derive the relationship between the dimensionless parameter, q^2b/EG, and the aspect ratio, h/b. Previous work has shown [6, 7] that this relationship can be characterized by a function $f(h/b)$. We find that $f(h/b)$ can be expressed as a polynomial with constant coefficients:

$$\frac{q^2b}{E} = Gf(h/b) \tag{4a}$$

$$f(h/b) = \frac{(h/b)^3}{a_1 + a_2(h/b)^2 + \frac{4(1-\nu^2)}{\pi}(h/b)^3 + a_3(h/b)^4} \tag{4b}$$

TABLE III Summary of parameters for $f(h/b)$

Theory	a_1	a_2	a_3
thin plate	$\frac{3}{32}(1-\nu^2)$	0	0
simple support	$\frac{3}{32}(7+\nu)(1-\nu)$	$\frac{3}{10}(1-\nu)$	$\frac{(-\nu^3+\nu^2+8\nu+524)}{2800}$
rigidly clamped	$\frac{3}{32}(1-\nu^2)$	$\frac{3}{10}(1+\nu)$	$\frac{(\nu^3-3\nu^2-312\nu+160)(1+\nu)}{840(1-\nu)}$
mixed	$\frac{3}{32}(7+\nu)(1-\nu)$	$\frac{(10+\nu)(1+\nu)}{40}$	$\frac{(\nu^3-3\nu^2-312\nu+160)(1+\nu)}{840(1-\nu)}$
thick plate	$\frac{3}{32}(1-\nu^2)$	$\frac{3}{8}(1+\nu)$	0

The values of a_1, a_2 and a_3 depend on the boundary conditions. Table III collects the various values from the different theories.

D. Final Relationship between *G* and Experimental Observables

By combining Eqs. (3) and (4) a simple formula for G emerges:

$$G = \frac{16Eh^3}{9(1-\nu^2)^2 R_c^2}\, g(h/b) \tag{5a}$$

$$g(h/b) = \frac{(h/b)^3}{fs^2} \tag{5b}$$

From this formula, we see that the theory splits into three multiplicative terms. The first term involves only E and ν, material parameters. The second term involves the experimentally determined variables, h and R_c. The third term, $g(h/b)$, is purely model dependent, accounting for the particular shape of the blister, and depends only on aspect ratio and ν. Equation (5) is the primary equation of the LIDS theory.

In Figure 3, a plot of $g(h/b)$ *versus* aspect ratio h/b is presented for the five sets of boundary conditions, where we have assigned $\nu = 1/3$ for convenience. Several features of the function are evident. First, aside from the thin plate theory, the theories are all close to one another, with a magnitude ~ 0.15. There are no discontinuities or large

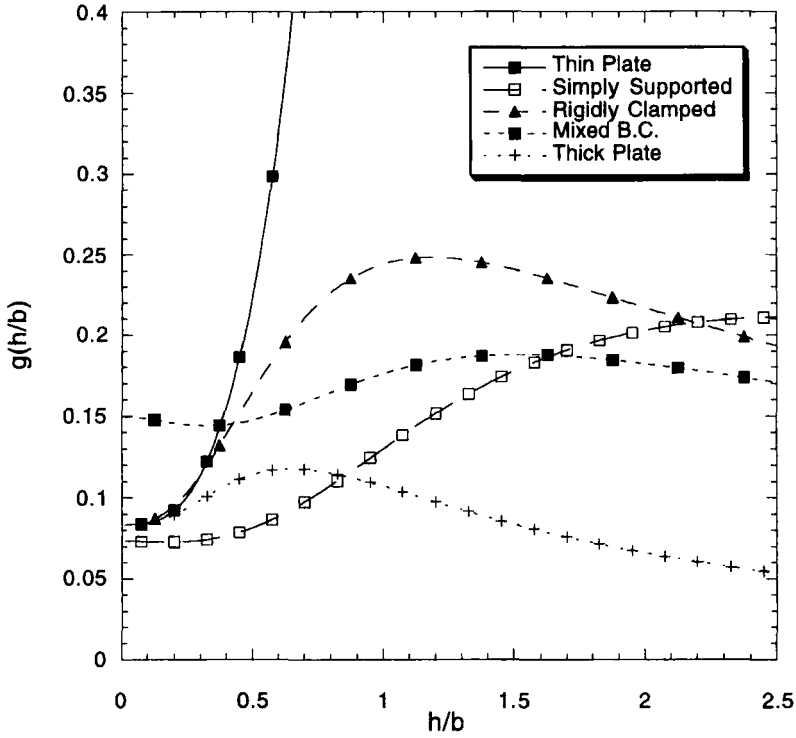

FIGURE 3 Comparison of the function $g(h/b)$ for various boundary conditions.

derivatives. As the aspect ratio of the experiment varies, the theoretical factor does not vary much at all. Thus, the LIDS experiment is very robust with respect to the theoretical analysis. On the practical side, when the LIDS experiment is performed the aspect ratio is usually between 0.5 and 1. This is because standard coating thicknesses just happen to result in this particular range of aspect ratios. In this study, $0.4 < h/b < 2.4$. In this range of aspect ratios, the mixed boundary condition case lies between the simply-supported and the rigidly-clamped cases. It is for this reason, along with our belief that it best describes the actual displacements, that we choose the mixed boundary condition case for the theoretical analysis. When data are analyzed using different theories, the absolute numbers do change, but the relationships between the values is preserved. It would be desirable to

see the problem solved with finite element analysis, but at this stage it is not clear how much true value would be gained from that endeavor.

It is possible to include the strain energy from the elastic foundation in the analysis. This leads to a small correction in Eq. (4). The correction is small because the deformation of the opaque polymer on the rigid substrate is small. It is also worth omitting this term because any theory would need to include the thickness of the layer along with its mechanical properties, E and ν. This introduces more variables into the equation for G, and does not contribute to the essence of the experiment. When LIDS is used to examine the adhesion between a coating and a thick (several millimeter) polymer substrate, we approximate the strain energy from the substrate in the constant term describing strain at the crack tip. So we use the strain energy at the crack tip to model all substrate conditions.

RESULTS

In Figure 4, we present a typical curvature *versus* pulse energy plot for a representative panel with black basecoat and 49.7 μm clearcoat,

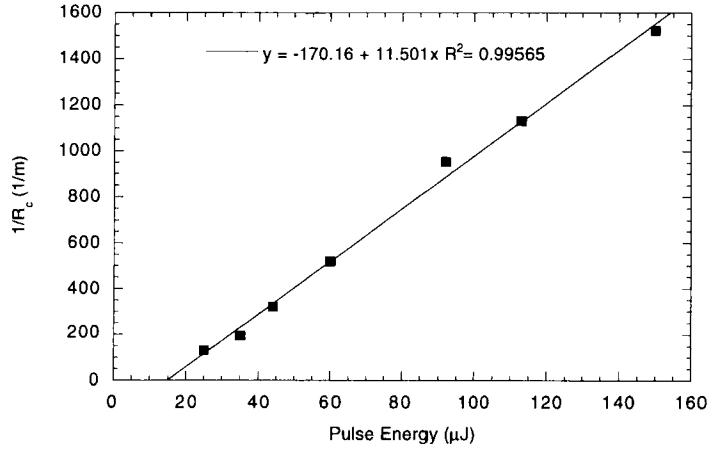

FIGURE 4 Experimental plot of measured curvature *versus* pulse energy, along with the best fit line.

along with a linear fit. The critical pulse energy at which debonding occurs in this sample is 150 μJ. We calculate the curvature at the critical pulse energy to be 1555 1/m, which corresponds to $G = 377\,J/m^2$, using Eq. (5). All results presented here have been analyzed using the mixed boundary condition case. For the work presented here, we take

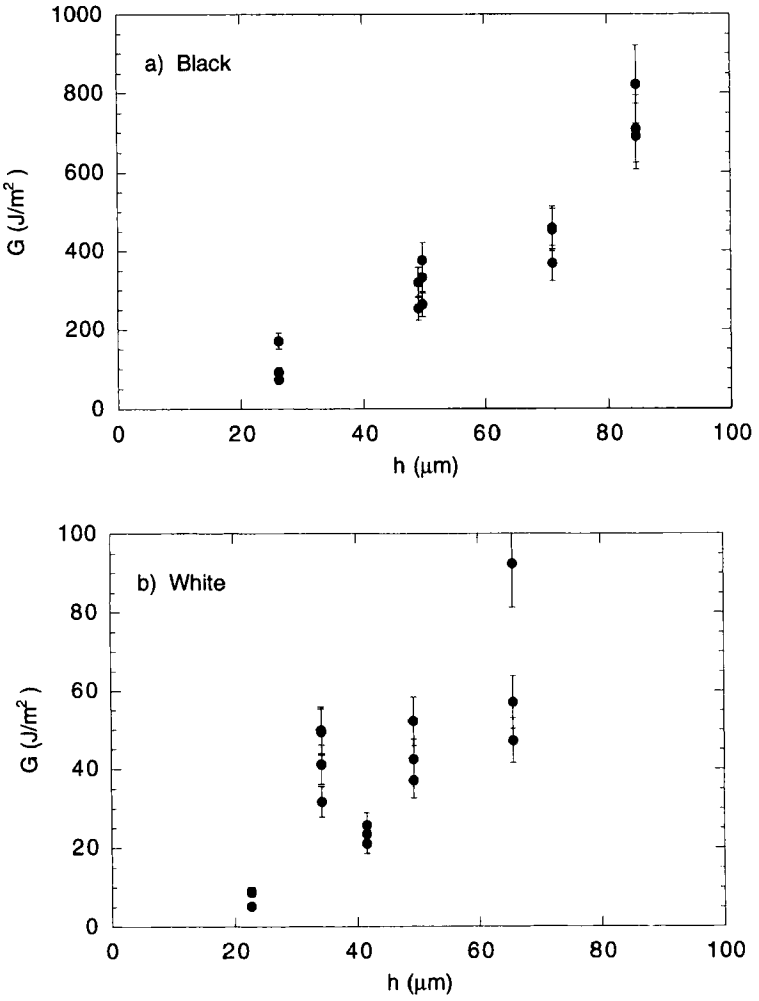

FIGURE 5 Plots of *G versus h* for the four basecoat colors studied: a) black; b) white; c) green; d) red.

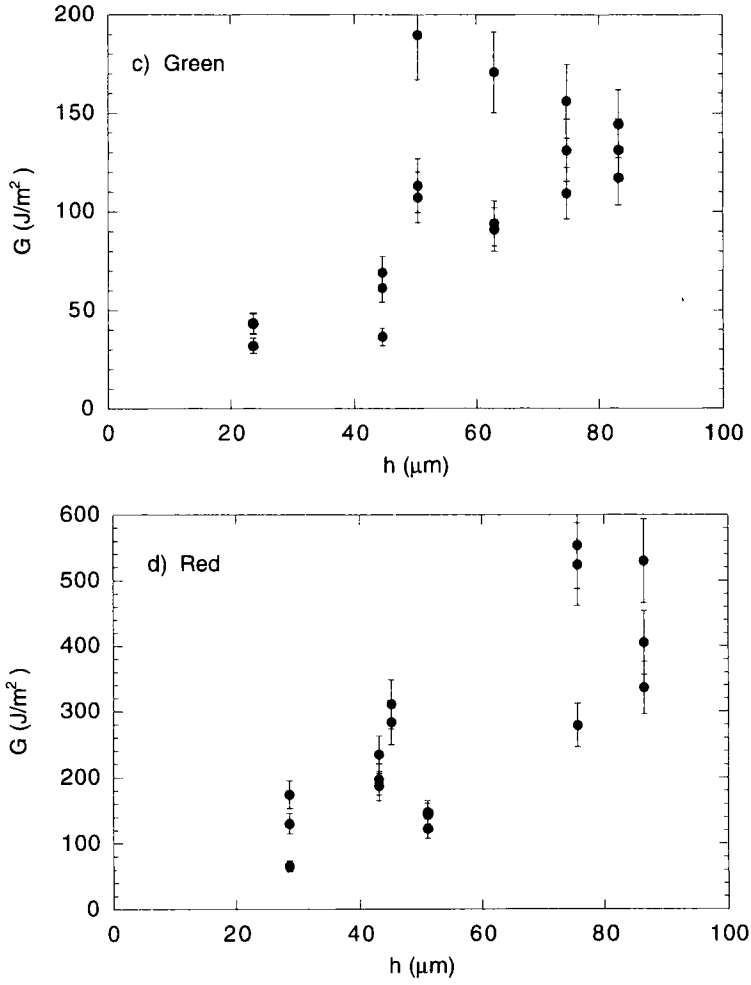

FIGURE 5 (Continued).

$E = 3\,\text{GPa}$ (from low temperature DMA measurements) and $\nu = 1/3$. For each coating thickness, three separate experiments were run on different regions of the plate to examine variations. In Figures 5a–d, we present G as a function of thickness of the transparent coating. Error bars of $\pm 12\%$ are included which represent the standard error.

This is derived from the error in R_c, which is usually $\sim 5\%$ and the error in thickness, which is 1% or less.

The first point to note is that G is not constant as the coating thickness varies. The adhesion is smaller for thinner coatings, and larger for thicker ones. This behavior is consistent with the existence of a plastic zone around the crack tip, the size of which is comparable with the coating thickness. If the coating was thicker than the plastic zone size, R_p, then G would be independent of thickness. As the coating thickness decreases, the plastic zone becomes truncated. Less energy is dissipated during the cracking process, and the measured value of G reflects this diminution [16]. By examining the data in Figure 5, we can estimate the size of the plastic zone by detecting this leveling in the value of G.

This range of behavior is seen in the data, from which we can empirically estimate the value of R_p. The black coating shows large values of G, along with G increasing with increasing thickness. Since there is no leveling off in G, we infer that $R_p > 85\,\mu m$ for this system, and $G = 740 \pm 41$ J/m^2 for that clearcoat thickness. For the red paint, we see that the G values for the two thickest specimens, 76 and 87 μm, are within error of each other. This observation leads us to believe that these thicknesses are greater than R_p. From this, we estimate $R_p \sim 70\,\mu m$. Below this thickness, the G value diminishes. For the two thickest clearcoats, the average value of adhesion is $G = 438 \pm 47$ J/m^2. Similarly for the metallic green paint, we estimate $R_p \sim 50\,\mu m$, and the average adhesion of the four clearcoats with $h > R_p$ is $G = 130 \pm 9$ J/m^2. Finally, for the white paint, we estimate $R_p \sim 30\,\mu m$, and the average value of the four thickest samples gives $G = 44 \pm 5$ J/m^2. The error bars represent one standard error. The results are summarized in Table IV.

TABLE IV Summary of LIDS results

Pigmentation	*PVC* (%)	G (J/m^2)	$R_p(\mu m)$ (*est.*)	$\sigma_y(MPa)$ (*est.*)
Black	3	740±41	> 85	> 39
Red	15	438±47	70	33
Metallic Green	7	130±9	50	22
White	21	44±5	30	16

DISCUSSION

To explain the differences in G between the various pigmented formulations, we must identify the differences between the coatings. The clearcoats are all identical, as are the electrocoat and primer. The only differences are in the basecoat. The resins comprising the basecoat are all the same. The only variation is the type and quantity of pigment, along with the small amount of polymeric pigment dispersant that must be included in the formulation. The type of pigment, along with its dispersant, will change the mechanical behavior of the sample in the small volume element surrounding the pigment (micromechanical behavior). The amount of pigment, in terms of pigment volume concentration (PVC), will determine the extent to which these micromechanical properties are manifested on the macroscopic scale.

Due to the preparative chemistry of organic pigments, the cohesive strength of such a pigment is not large. The pigment particles are essentially flawed microcrystals. Thus, the weakest part of the basecoat, when considering a concept such as cohesive energy density, is at the boundary between the pigment and the host polymer matrix, or within the pigment itself. The pigment/matrix interface is mediated by a special polymeric dispersant, which is different for each pigment. Thus, different formulations have different pigment/matrix interfacial strengths.

TEM and XPS studies have shown that the locus of failure between basecoat and clearcoat due to accelerated weathering occurs not at the boundary between the two coatings, but rather a few microns from the interface, inside the basecoat [17]. We assume that this analysis holds true for the LIDS experiment, also. Thus, the G value measured in this LIDS experiment is mostly a measure of the cohesive strength of the basecoat at high strain rates. This strength is primarily determined by the strength of the pigment/matrix boundary layer, and by the total amount of pigment/matrix interfacial area (related to PVC).

With this approach, we can understand the LIDS results. The black formulation has the highest adhesion because it has the lowest PVC and because carbon black, the pigment, can be easily dispersed into these systems. The aromatic nature of carbon black, along with the high energy of orbitals at the edge of each pigment molecule, provides

a relatively strong pigment/matrix boundary layer. The white formulation has the lowest adhesion. The large PVC probably accounts for most of the variation. The strength of the pigment/matrix interaction is probably less than for an organic pigment, but this has not been proven yet. The relatively large value of G for the red formulation leads to the conclusion that the pigment/matrix boundary layer is relatively strong for this material, since the PVC is relatively high. Indeed, one would expect a high surface energy for these quinacridone pigments which contain oxygen and nitrogen atoms in their structure. The high surface energy would increase the pigment/matrix interfacial strength. Finally, the metallic green formulation is unique. The PVC of 7% is composed of 3% organic pigment and 4% aluminum flakes. The high aspect ratio of the aluminum flakes leads to a large pigment/matrix surface area. So for this relatively low PVC, there must be a weak boundary layer between the aluminum flake and the matrix to explain the low value of G.

It is clear that consideration of just PVC is not enough to account for the variation in G. However, the concept that cohesive strength of the basecoat is the most influential factor is worth pursuing. To this end, there is ongoing research within our organization to measure properties such as tensile strength on these coatings.

As a minor effect, inclusion of pigment will change the modulus of the basecoat. However, since the modulus is associated with nondissipative processes, it will not affect the practical work of adhesion to a significant degree. To a first approximation, the modulus will be the weighted average of the components in the system. For black and red pigmentations, which are organic pigments, there will be no significant change. For the white there should be an increase, and for the green there would be an increase due to the presence of aluminum.

LIDS is not the first quantification of paint adhesion. This has been accomplished previously using the inverted blister test [10]. In that work, Kinloch and coworkers measured the adhesion between electrocoated paint (epoxy-amine) and a steel substrate to be $G = 100\,\mathrm{J/m^2}$. This value compares favorably with the values being measured in this work. Albeit for a different system, it helps to benchmark our results.

From the data, we can derive an effective yield stress around the crack tip using the formula relating R_p with the yield stress and stress

intensity factor for plane strain [16, 18]:

$$R_p = \frac{EG}{6\pi(1-\nu^2)\sigma_y^2} \tag{6a}$$

$$\sigma_y^2 = \frac{EG}{6\pi(1-\nu^2)R_p} \tag{6b}$$

We can use our estimates of R_p along with the measured values of G to deduce the effective yield stress in these systems. We find that $\sigma_y = 16$ MPa for white, 22 MPa for green, 33 MPa for red, and > 39 MPa for black. The magnitudes of these values are consistent with model predictions for the yield stress in polymer systems [19].

The blister's curvature is not independent of time. The blister relaxes back to the surface of the plate over time (to within the surface noise of the plate as examined by microscopic white light interferometry) for energies below critical. Once the energy is over critical, and the sample is fractured, complete relaxation does not occur. We have performed LIDS between a thin glass plate (50 μms thick, from Schott glass) and a black epoxy substrate. These experiments were useful because the glass plate was not susceptible to plastic deformation. From these experiments, we were able to determine the time dependence of the pressure in the blister. We found that the pressure decays exponentially with a decay time of ~ 1 ms. When we performed the clearcoat-basecoat experiments, we saw that the time dependence of the blister varies. At low pulse energies, where the blister is small and plastic deformation is small, we see that the curvature of the blister decays on a millisecond time scale, similar to the glass plate. As the laser pulse energy is increased, the decay time also increases and becomes non-exponential, due to viscoelastic processes in the polymer. For higher pulse energies, we have followed the blister relaxation over 10 decades of time, from 10^{-5} s to 10^5 s, and are working on relating this time dependence to the relaxation spectrum of the polymer. In the experiments presented here, we measured the blister curvature for the first 10 μs. On this time scale it is constant, which enables us to measure the initial curvature from the ablation event.

The temperature rise in the sample is not a major concern in the LIDS experiment because the process occurs much faster than thermal

diffusion. The opaque layer heats up and ablates, and the regions that do not ablate also heat up, but only by a small amount. The transparent layer does not heat up. On the time scale of the experiment, $\sim 1\,\mu s$, heat can diffuse in a polymer only $\sim 1\,\mu m$. Therefore, the transparent coating, which is tens of microns, is not heated. The strain in the sample is a few percent, so the strain rate of LIDS is $\sim 10^5$. This high strain rate reduces the effect of increased temperature.

There are several parts to the LIDS experiment that can be improved. First, the HeNe laser samples a finite region of the blister, and does not measure the curvature at the exact center. This can be improved by further reduction in the HeNe spot size, or by taking into account the nonparabolic nature of the reflecting surface in the Gaussian beam propagation equations. Second, the experiment takes more effort to perform than the crosshatch-peel test, and concomitantly more time. Thus, LIDS is good for performing quantitative studies on the nature of coating adhesion, but probably would not be convenient as an everyday test method. The theoretical analysis can be improved by examining the deformation in more detail, using finite element analysis, but the current analysis is fairly robust. There is also a range of thicknesses of the transparent polymer over which LIDS will work, depending on G and the modulus of the coating. If the polymer is too thin ($\sim 10\,\mu m$ for these films), then the blister shears off from the substrate before crack propagation begins. If the polymer is too thick (we have successfully performed LIDS on samples with thicknesses of $150\,\mu m$), then the curvature of the top surface will become too small to detect accurately.

There are many advantages to the LIDS experiment. Foremost, the experiment works on samples directly from the field or automotive testing laboratory. It works on the fender of a typical automobile. Samples may be examined without drilling holes in the specimen, or adhering it to other substrates. We find good correlations between the LIDS results and those from crosshatch-peel tests and gravelometer testing. We are able to examine samples that have been subjected to accelerated aging. While the results presented here are for clearcoat-basecoat adhesion, we can use LIDS to examine other interfaces, too. By removing the pigment from a basecoat, and leaving off the topcoat, we can examine the adhesion between primer and basecoat.

Similarly, we can examine the adhesion between an unpigmented primer and electrocoat, and between an unpigmented coating and a substrate such as thermoplastic olefin, copper, steel, or reactive injection-molded polymers. We are able to quantify the effects of baking conditions, formulation variables, and aging on coating adhesion, which enables us to direct development to more robust coating systems.

CONCLUSIONS

We have demonstrated how the LIDS technique may be used to derive the practical work of adhesion for systems consisting of a transparent polymer coated onto an opaque polymer supported by a rigid substrate. The adhesion between an automotive clearcoat and four different colored basecoats has been measured, and we find that the black has the strongest initial adhesion, while the white has the weakest, and the red and green intermediate. Although approximate analytic models were used, the derived values of the adhesion parameter could be bounded by these models, and the results are qualitatively unchanged. The differences in adhesion can be accounted for by the various pigmentations.

Acknowledgements

JSM would like to thank A. J. Kinloch, J. G. Williams, and A. Jagota for many helpful discussions throughout the development of this work.

References

[1] Mittal, K. L., Ed., *Adhesion Measurement of Films and Coatings* (VSP, Utrecht, 1995).
[2] Anderson, G. P., Bennett, S. J. and DeVries, K. L., *Analysis and Testing of Adhesive Bonds* (Academic, New York, 1977).
[3] Lambourne, R., Ed., *Paint and Surface Coatings: Theory and Practice* (Ellis Horwood, Ltd., West Sussex, England, 1987).
[4] Dannenberg, H., *J. Appl. Polym. Sci.* **5**, 124 (1961).
[5] Williams, M. L., *J. Appl. Polym. Sci.* **13**, 29 (1969).
[6] Bennett, S. J., DeVries, K. L. and Williams, M. L., *Int. J. of Fracture* **10**, 33 (1974).

[7] Andrews, E. H. and Stevenson, A., *J. Mat. Sci.* **13**, 1680 (1978).
[8] Allen, M. G. and Senturia, S. D., *J. Adhesion* **25**, 303 (1988).
[9] Chang, Y., Lai, Y. and Dillard, D. A., *J. Adhesion* **27**, 197 (1989).
[10] Fernando, M., Kinloch, A. J., Vallerschamp, R. E. and van der Linde, W. B., *J. Mat. Sc. Letts.* **12**, 875 (1993).
[11] Griffith, A. A., *Phil. Trans. Royal Soc.* **221**, 163 (1921).
[12] Siegman, A. E., *Lasers* (University Science Books, Mill Valley, CA 1986).
[13] Timoshenko, S. and Goodier, J. N., *Theory of Elasticity* (McGraw-Hill, New York, 1970).
[14] Timoshenko, S. and Woinowsky-Krieger, S., *Theory of Plates and Shells* (McGraw-Hill, New York, 1959), p. 74.
[15] Sneddon, I. N. and Lowengrub, M., *Crack Problems in the Classical Theory of Elasticity* (Wiley, New York, 1969), p. 134.
[16] Kinloch, A. J., *Adhesion and Adhesives: Science and Technology* (Chapman and Hall, London, 1987), Chap. 7.
[17] Barbara Wood and Kate Stika, private communications.
[18] Williams, J. G., *Fracture Mechanics of Polymers* (Ellis Horwood, Ltd., West Sussex, England, 1984), Chap. 5.
[19] Bicerano, J., *Prediction of Polymer Properties* (Marcel Dekker, New York, 1993), Chap. 11.

APPENDIX A

In this section we detail the extraction of the curvature of the blister from the intensity of the HeNe laser [12]. The HeNe laser can be successfully modeled as a Gaussian beam defined at any point by a beam diameter, w, and radius of curvature of the wavefront, R, whose initial values are w_0 and R_0, respectively. Each optical element, be it a lens or a mirror, affects these two parameters in a known way. The variable q, not to be confused with the blister pressure, is a complex quantity characterizing the curvature and spot size of the laser by the following relation:

$$\frac{1}{q_0} = \frac{1}{R_0} + \frac{1}{iz_0} \tag{A.1}$$

where $z_0 = \pi w_0^2/\lambda$, and wavelength $\lambda = 632.8\,\text{nm}$. Since the beam is initially collimated, q_0 is a purely imaginary parameter. In the LIDS experiment, the beam then propagates a distance d_0 to a lens of focal length $f = 100.0\,\text{mm}$. The beam then focuses through a distance d_2 to the sample, where it reflects from the surface possessing a radius of curvature R_c, which we wish to determine. The beam then propagates

through a distance d_4 to the aperture, where its spot size is measured. These steps are summarized by the relations:

$$q_1 = q_0 + d_0 \tag{A.2}$$

$$\frac{1}{q_2} = \frac{1}{q_1} - \frac{1}{f} \tag{A.3}$$

$$q_3 = q_2 + d_2 \tag{A.4}$$

$$\frac{1}{q_4} = \frac{1}{q_3} + \frac{2}{R_c} \tag{A.5}$$

$$q_5 = q_4 + d_4 \tag{A.6}$$

By continued substitution, one arrives at an expression for q_5:

$$\begin{aligned} q_5 = d_4 &\left((f - d_0 - q_0) + \frac{2}{R_c}(d_2(f - d_0 - q_0) + f(d_0 + q_0)) \right) \\ &+ (d_2(f - d_0 - q_0) + f(d_0 + q_0))/(f - d_0 - q_0) \\ &+ \frac{2}{R_c}(d_2(f - d_0 - q_0) + f(d_0 + q_0)) \end{aligned} \tag{A.7}$$

and the beam spot size is related to q_5 by:

$$w = \left(\frac{-\lambda}{\pi Im(1/q_5)} \right)^{1/2} \tag{A.8}$$

The intensity of light from a Gaussian laser beam passing through a circular aperture is given by the equation:

$$\frac{I}{I_0} = 1 - \exp\left[-2\frac{a^2}{w^2} \right] \tag{A.9}$$

where a is the radius of the aperture and I is the intensity. In the LIDS experiment, we measure this intensity ratio, invert Eq. (A.9) to get w and hence q_5. Equation (A.7) is inverted to solve for R_c:

$$\frac{1}{R_c} = \frac{(2\pi/\lambda) f w_0 (w^2 k - 4d_4^4 f^2 w_0^2)^{1/2} - m}{2k} \tag{A.10}$$

where

$$m = 4d_4(f^2(d_2^2 + d_2\,d_4 + d_0\,d_4) + (f - d_2 - d_4)\\ (2f\,d_0\,d_2 - (d_0^2 + z_0^2)(d_2 - f))) \tag{A.11}$$

and

$$k = 4\,d_4^2\,\{(d_2 - f)^2 z_0^2 + (f\,[d_0 + d_2] - d_0\,d_2)^2\} \tag{A.12}$$

These equations allow us to convert from intensity passing through a pinhole to the curvature of the blister.